Materials Chemistry and Physics 172 (2016) 77–86

Contents lists available at ScienceDirect

Materials Chemistry and Physics

journal homepage: www.elsevier.com/locate/matchemphys

Investigation of structural, electronic, and optical properties of the monoclinic and triclinic polymorphs of hexamethylenetetraminium 2,4-dinitrophenolate monohydrate ($C_6H_{13}N_4^+ \cdot C_6H_3N_2O_5^- \cdot H_2O$) compound: A DFT approach

Zeyad A. Alahmed [a, *], A.H. Reshak [b, c], Suchada Chantrapromma [d], Hoong-Kun Fun [e]

[a] Department of Physics and Astronomy, College of Science, King Saud University, Riyadh 11451, Saudi Arabia
[b] New Technologies-Research Center, University of West Bohemia, Univerzitni 8, Pilsen 306 14, Czech Republic
[c] Center of Excellence Geopolymer and Green Technology, School of Material Engineering, University Malaysia Perlis, Kangar 01007, Perlis, Malaysia
[d] Department of Chemistry, Faculty of Science, Prince of Songkla University, Hat-Yai, Songkhla 90112, Thailand
[e] Department of Pharmaceutical Chemistry, College of Pharmacy, King Saud University, Riyadh 11451, Saudi Arabia

HIGHLIGHTS

- Electronic and optical properties of two phases of polymorphs were studied by DFT.
- The monoclinic polymorph possess an indirect band gap of 1.935 eV using (PBE-GGA).
- The triclinic polymorph has an indirect band gap of 1.773 using (PBE-GGA).
- The monoclinic and triclinic phases exhibit a wide optical transparency region.

ARTICLE INFO

Article history:
Received 25 July 2015
Received in revised form
1 December 2015
Accepted 30 December 2015
Available online 8 January 2016

Keywords:
Optical materials
Organic compounds
Electronic materials
Ab initio calculations
Band-structure

ABSTRACT

We have investigated the structural, electronic and optical properties for two phases of polymorphs of hexamethylenetetraminium 2,4-dinitrophenolate monohydrate ($C_6H_{13}N_4^+ \cdot C_6H_3N_2O_5^- \cdot H_2O$) compound which were synthesized by Hoong-Kun Fun's group. The first phase possesess monoclinic $P2_1/m$ space group, while the other phase has triclinic P1 space group. The all electron full potential linearized augmented plane wave (FP-LAPW + lo) method within the local density approximation (LDA) and the Perdew-Burke-Ernzerhof generalized gradient approximation (PBE-GGA) were used. Calculation shows that the conduction band minimum (CBM) for the two phases is located between D and Z points of the Brillouin zone (BZ) while the valence band maximum (VBM) is located at the center of the BZ, resulting in an indirect band gap. It has been found that the monoclinic (300 K) polymorph possesses a band gap of about 1.884 (LDA) and 1.935 (PBE-GGA) eV while triclinic (143 K) polymorph has a band gap of about 1.720 (LDA) and 1.773 (PBE-GGA) eV. For a deeper insight into the electronic structure, we have performed comprehensive optical properties calculations. These confirm the band gap reduction during the phase transition (300 K→143 K). The bond lengths and angles are calculated and compared with the experimental data; good agreement was found which reveals the accuracy of the calculations.

1. Introduction

Crystals having different arrangements of the same elements/compounds in their unit cells are called allotropes/polymorphs respectively. More precisely, allotropes/polymorphs are crystals comprising the same elements/compounds but crystallizing out in different space groups. Allotropes/polymorphs have the same chemical properties but different physical properties. An excellent example is given by the different physical properties of the two allotropes of carbon, namely, graphite and diamond. Polymorphism can occur with inorganic, organic and biological compounds as well as in proteins. In pharmacy, polymorphism plays a very crucial role

* Corresponding author.
E-mail address: zalahmed@ksu.edu.sa (Z.A. Alahmed).

http://dx.doi.org/10.1016/j.matchemphys.2015.12.063
0254-0584/

in commercial drugs and medicines, some polymorphs being more effective than others, for example in their solubility in the blood stream.

2,4-Dinitrophenol or DNP which is also sold as Dinosan, Chemox or Sulfo Black, is promoted as a weight-reducing agent that causes rapid and significant weight loss. In bodybuilding, it is used as a diet pill for rapid fat loss, but it is considered extremely dangerous when ingested, and this use was stopped in 1938 [1]. It was also used as an antiseptic, herbicide, pesticide, explosive, manufacture of dyes and wood preservatives. Although DNP does cause weight-loss, because of its association with death its use cannot be recommended under any circumstances. Even though in the 1930s, the US Food and Drug Administration determined that DNP was "extremely dangerous and not fit for human consumption". But up to now it is appeared that there has been increasing interest and availability of DNP-containing products on the internet. Whilst these appear to be largely targeted towards bodybuilders to try and reduce fat and improve muscle bulk, there have been a number of deaths related to its use for more general weight loss [2]. DNP can be absorbed through skin or lungs which caused weight loss, weakness, dizziness and excess sweating. In some cases the patient would die, with body temperatures rising to over 40°, maybe as high as 43–44 °C. DNP works via increasing heat production in cells via a process known as uncoupling (making cells less efficient with energy) and small overdoses have been known to result in death. The poisoning of DNP is well documented [2–5], the acute (short-term) effects of DNP in humans through oral exposure are nausea, vomiting, sweating, dizziness, headaches, and loss of weight. Chronic (long-term) oral exposure to DNP in humans has resulted in the formation of cataracts and skin lesions, weight loss, and has caused effects on the bone marrow, central nervous system (CNS), and cardiovascular system. EPA (United States Environmental Protection Agency) classified DNP as a high acute toxicity substance.

Hexamethylenetetramine or HMT is a heterocyclic compound which is useful in the synthesis and many applications such as plastics [6], pharmaceuticals [7] and rubber additives [8,9]. In medicine, HMT is typically used as a long-term urinary antiseptic and to prevent the recurrence of infections. Its anti-infective action derives from the slow release of formaldehyde, a nonspecific bactericidal agent, by hydrolysis at acidic pH [10]. Due to the usages of both DNP and HMT in pharmaceuticals and food, the drug–drug or drug–food interactions can be occurred. The drug interactions can cause the medications to be less or more potent than intended. They can also result in unexpected side effects, which may be harmful. The previous report also showed that the HMT in the present of DNP was useful in the rubber vulcanization [9]. In addition Fun et al., 2003, reported that phenol–amine adducts of DNP-HMT exhibited phase transition due to hydrogen bond which was explained by ferroelastic theory [11]. These importance of both DNP and HMT in food, pharmaceutical and materials has led us to study some other properties which are structural, electronic and optical properties of DNP-HMT adducts by DFT approach.

Polymorphs are divided into two categories, monotropes and enantiotropes, depending upon their stability with respect to the range of temperatures and pressures. The first category of polymorphs is stable over a certain temperature range and pressure, while the second category of polymorphs is stable over different temperature ranges and pressures; these polymorphs are known as enantiotropes. On the other hand, sometimes only one polymorph is stable at all temperatures below the melting point whereas all the other polymorphs are unstable. Each such polymorph is known as a monotrope. The overall properties and usefulness of polymorphs have been described in an article on polymorphism [12].

It has been reported by Usman et al. [13] that 3,5,7-triaza-1-azoniatricyclo[3.3.1.1^{3,7}]-decane 2,4-dinitrophenolate monohydrate, undergoes a temperature phase transition from a monoclinic to a triclinic polymorph. The difference between the two polymorphs is in the packing, which is governed by the different hydrogen bonding and weak interaction patterns. Therefore, they attributed the reversible temperature phase transition to the presence or absence of the extra hydrogen bonding and weak interactions [13].

The crystal structures of the 143 and 300 K polymorphs of the organic compound, hexamethylenetetraminium 2,4-dinitrophenolate monohydrate **(I)**, have been solved [13]. A temperature-dependent study reveals the ferroelastic phase transition temperature to be $T_c = 260$ K. This ferroelastic phase transition has been explained macroscopically by Landau Theory [14] and microscopically using a pseudo-spin Hamiltonian based on the interaction between the hydrogen bonds and the lattice phonons [15,16]. Several other organic compounds which exhibited phase transition have also been reported [17–20].

Since polymorphs have different physical properties, it would be interesting to investigate the physical properties of the two polymorphs of **(I)**. Thus, it motivates us to focused our attention on utilize the density functional theory (DFT) within the full potential method to deduce the electronic and optical properties of the two enantiotropes of **(I)**, making use of the molecular geometry of the two polymorphs of **(I)** obtained from the x-ray crystallographic data.

In this article, we described the computational methods in Section 2, whereas in Section 3, we discuss the structural properties, electronic, and optical properties of the two polymorphs of **(I)**. In the last section we have summarized the result of this work.

2. Computational details

We have used the all-electron full-potential linearized augmented plane wave plus local orbitals (FP-LAPW + lo) method as implemented in the WIEN2k package [21] to solve the Kohn Sham equations [22]. The structural, electronic band structures and optical properties of the monoclinic and triclinic phases were calculated using the minimum radius of the muffin-tin spheres (R_{MT}) values for O, N, C and H atoms in the monoclinic (triclinic) phase as 0.89 (1.06), 1.07 (0.96), 1.03 (1.09) and 0.48 (0.52) a.u., respectively. These values were chosen to ensure that there is no charge leakage out of the atomic sphere cores. The local density approximation (LDA) [23] and Perdew-Burke-Ernzerhof generalized gradient approximation (PBE-GGA) [24] were used to treat the exchange and correlations potentials. To achieve an accurate result the X-ray diffraction data obtained by Usman et al. [13] were optimized. Relaxed atomic positions were obtained by minimizing the forces (1 mRy/a.u.) acting on each atom. The results show that the maximum differences between the calculated and experimental values are less than 2.3×10^{-3} (1.8×10^{-3}) (Å) in the unit of the primitive cell for the monoclinic (triclinic) phase, which reveals the accuracy of the calculations.

The plane wave cut off parameters were decided by $R_{MT}K_{max} = 7$, $l_{max} = 10$, and $G_{max} = 30$ (a.u.)$^{-1}$ for a Fourier expansion of the change density. The separation parameter between the valence and core states was estimated to be −6.0 Ry. The self consistency for monoclinic phase is obtained using 90 **k**-points in the irreducible wedge of the first Brillouin zone (IBZ) while 85 **k**-points are taken in IBZ for triclinic phase. The self-consistent calculations are considered to have converged when

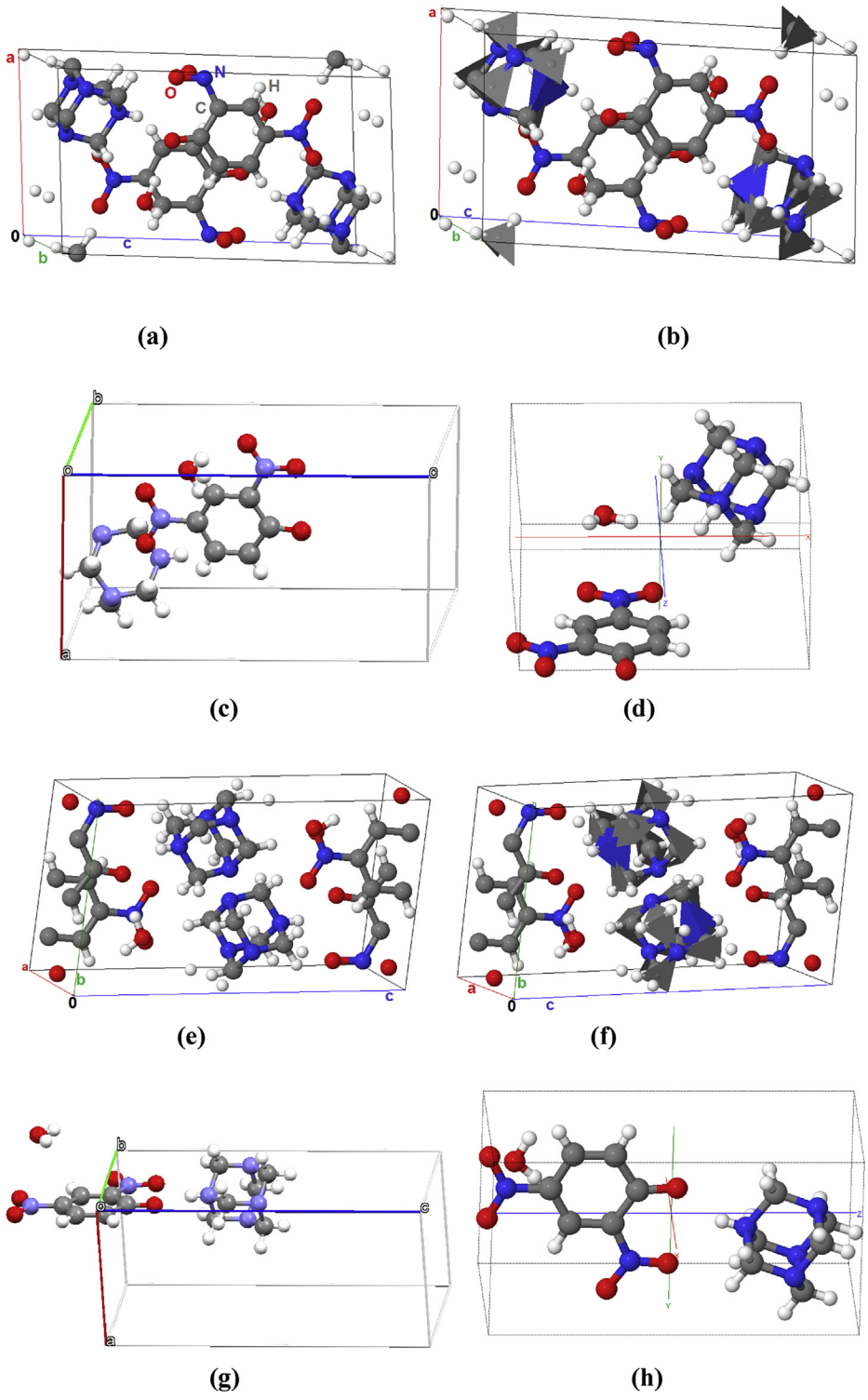

Fig. 1. The crystal structures for; (a) unit cell of the monoclinic structure (monoclinic); (b) unit cell of the monoclinic structure (monoclinic) show the polyhedron; (c) The asymmetric unit of the monoclinic structure contains one half of a hexamethylenetetramine molecule. One half of the hexamethylenetetramine molecule is related to the other by a centre of symmetry; (d) single molecule of the monoclinic structure; (e) unit cell of the triclinic (triclinic) of polymorphs; (f) unit cell of the triclinic (triclinic) of polymorphs show the polyhedron; (g) The asymmetric unit of the triclinic structure contains a hexamethylenetetramine molecule; (h) single molecule of the triclinic structure.

the total energy is stable within 10^{-5} Ry.

The electronic band structure and density of states of monoclinic (triclinic) phases were calculated using 90 (85) **k**-points in the irreducible wedge of the first Brillouin zone (IBZ).

We have calculated the linear optical properties of the monoclinic and triclinic phases using PBE-GGA to get deeper insight into the electronic structure. The optical properties were calculated using the optical program incorporated in WIEN2k package [21].

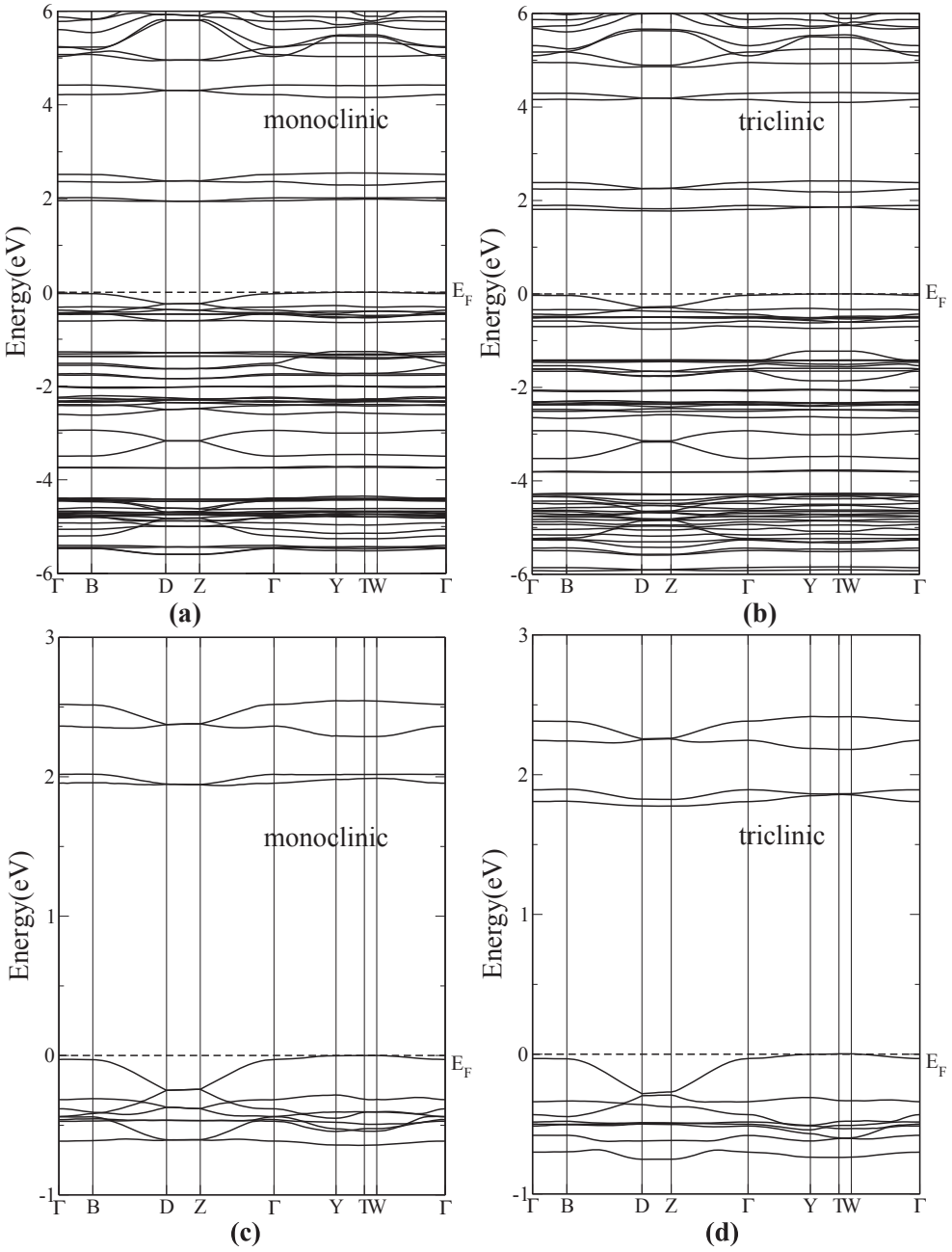

Fig. 2. The calculated band structure using PBE-GGA for (a) monoclinic phase; (b) triclinic phase of the titled compound; (c) enlarged band structure around E_F in the energy range between (−1.0 and 3.0) eV for the monoclinic phase; (c) enlarged band structure around E_F in the energy range between (−1.0 and 3.0) eV for the triclinic phase.

According to the symmetry therefore, both phases have three non-zero components of dielectric tensors. These are $\varepsilon^{xx}(\omega)$, $\varepsilon^{yy}(\omega)$ and $\varepsilon^{zz}(\omega)$, based on the electric field components $\vec{E}$ along the lattice vectors of the primitive cell. The imaginary parts $\varepsilon_2^{xx}(\omega)$, $\varepsilon_2^{yy}(\omega)$ and $\varepsilon_2^{zz}(\omega)$ of the optical dielectric function are calculated in terms of the Fermi distributions of the conduction f_c and valence bands and f_v using the expression given in reference [25]:

$$\varepsilon_2^{ij}(\omega) = \frac{8\pi^2\hbar^2e^2}{m^2V}\sum_k\sum_{cv}(f_c - f_v)\frac{p_{cv}^i(k)p_{vc}^j(k)}{E_{vc}^2}\delta[E_c(k) - E_v(k) - \hbar\omega]$$

where $\hbar$, e, m and V are the Planck's constant, charge, electron mass and the unit cell volume, respectively. The momentum matrix element transition from the energy level c of the conduction band to the level v of the valence band at certain **k**-point in the BZ and V is given by the term $p_{cv}^i(k)$. The real parts $\varepsilon_1^{xx}(\omega)$, $\varepsilon_1^{yy}(\omega)$ and $\varepsilon_1^{zz}(\omega)$ can be determined from the imaginary parts using Kramers-Kronig transformation [25]. The optical properties of monoclinic (triclinic) phases were calculated using 90 (85) **k**-points in the irreducible wedge of the first Brillouin zone (IBZ). The linear optical properties are calculated using the optical code implemented in WIEN2k package [21], for more details please see the user guide [26] and ref. [25]. We would like to mention here that we have used Grace package [27] to plot the band structures, density of states and optical properties. While the electronic charge density is plotted using

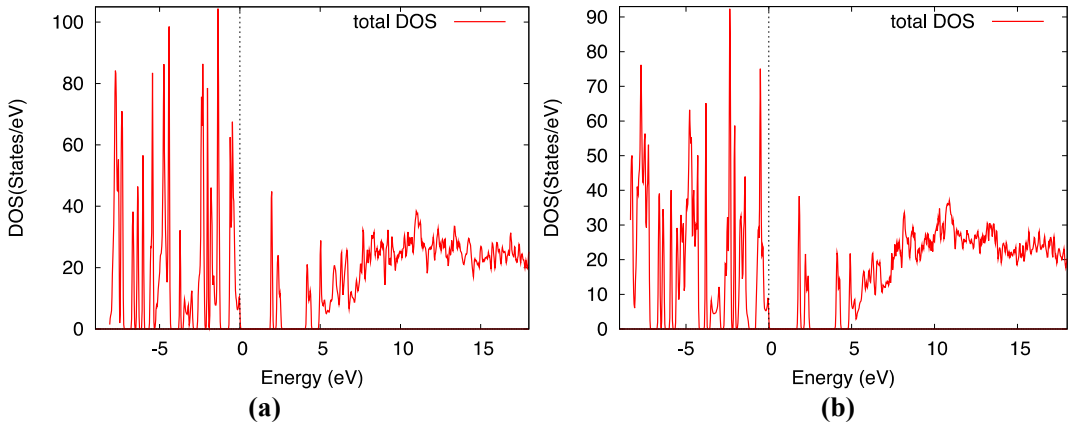

Fig. 3. The calculated total density of states (States/eV) for (a) monoclinic (monoclinic) and (b) triclinic (triclinic) phases of the titled compound using PBE-GGA.

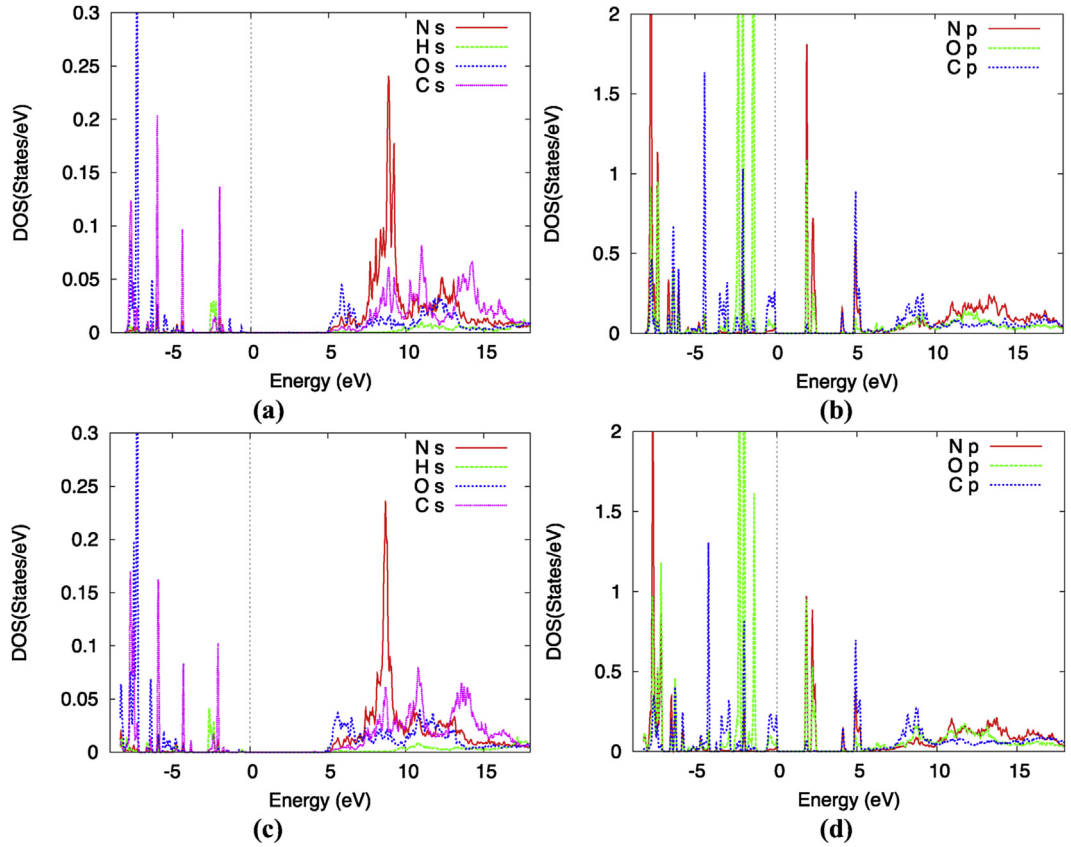

Fig. 4. The calculated partial density of states (States/eV) for (a,b) monoclinic (monoclinic) and (c,d) triclinic (triclinic) phases of the titled compound using PBE-GGA.

XCrysden package [28].

3. Results and discussion

3.1. Structural properties

It has been reported that ($C_6H_{13}N_4^+.C_6H_3N_2O_5^-.H_2O$) compound crystallizes in two phases [13]. The first phase crystallizes in monoclinic space group $P2_1/m$ (No. 11). The unit cell volume is 745.89 Å^3, with unit cell parameters a = 7.8610 Å, b = 6.5980 Å, c = 14.4339 Å, $\alpha = \gamma = 90°$, $\beta = 94.915°$ and z = 2 [13]. Whereas the second phase exhibited triclinic space group P $\bar{1}$ (No. 2). The unit cell volume of triclinic phase is 722.11 Å^3, with unit cell parameters a = 6.3877 Å, b = 7.9017 Å, c = 14.4042 Å, α = 84.4120°, $\beta = 86.3670°$, $\gamma = 89.3040°$ and z = 2 [13]. The crystal structures of these two phases were presented in Fig. 1.

The experimental structure parameters of monoclinic and triclinic phases were used in the present computational study, subject to optimization of the internal coordinates by minimizing the forces acting on each atom, keeping the lattice constants, angles and the unit cell volumes fixed at the experimental values. We assume that the structure is totally relaxed when the forces on each atom reach values less than ($1mRy/a.u.$). The resulting relaxed internal coordinates are used to calculate the ground state properties.

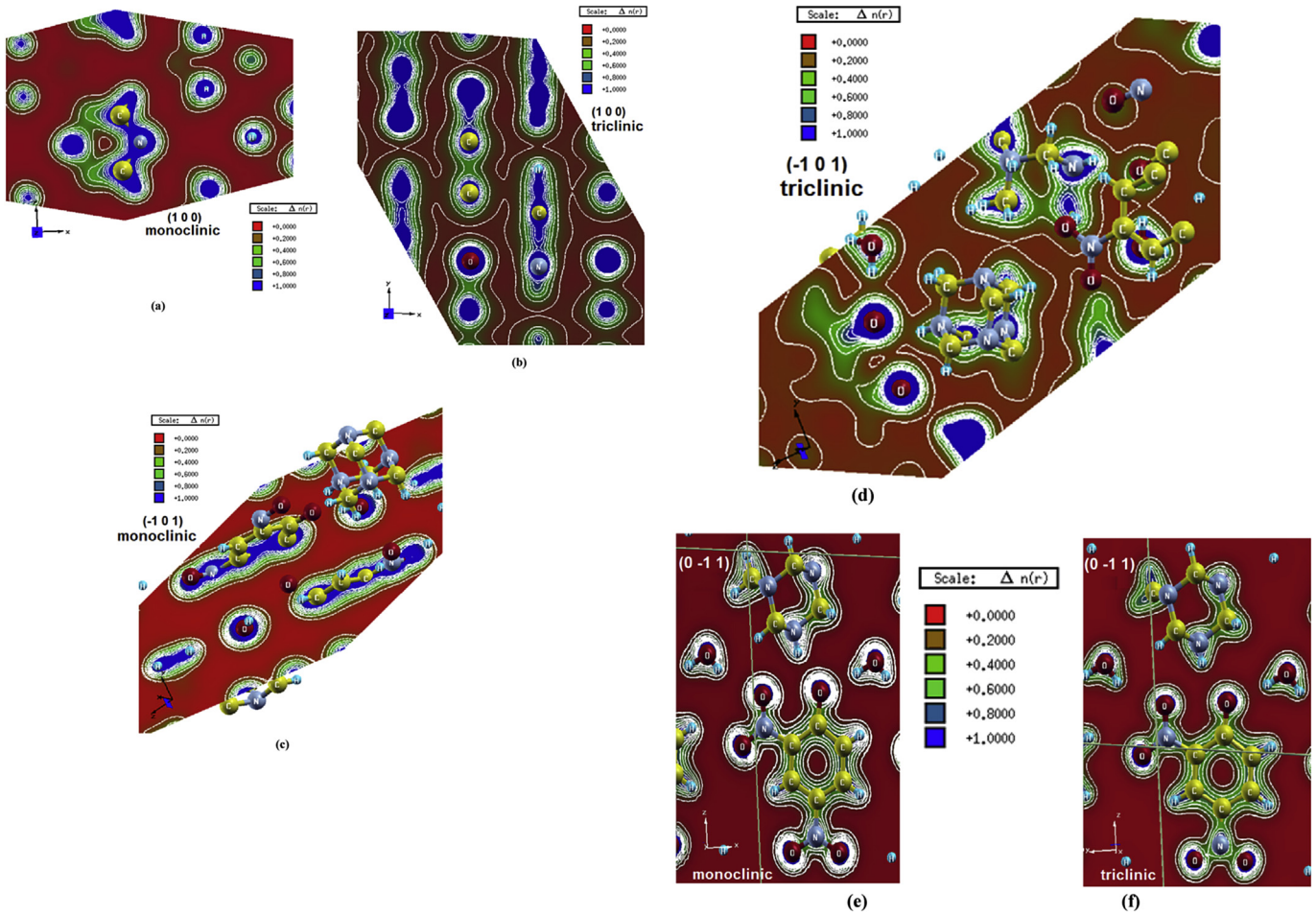

Fig. 5. The electronic charge density contour for (a) the (1 0 0) plane of monoclinic phase; (b) the (1 0 0) plane of triclinic phase; (c) the (−1 0 1) plane of monoclinic phase; (d) the (−1 0 1) plane of triclinic phase; (e) the (0−1 1) plane of monoclinic phase; (f) the (0−1 1) plane of triclinic phase. These calculations were performed using PBE-GGA.

The relaxed internal coordinates are presented in Table S1 and Table S2 in comparison with the experimental data, good agreement was found.

3.2. Electronic properties

3.2.1. Band structures

The calculated electronic band structures along the high symmetry points Γ (0 0 0), B (0.5 0.5 0.5), D (0.5 0 0), Z (0 0 0.5), Γ (0 0 0), Y (0.5 0.5 0), T (0.5−0.5 0), W (0.5 0 0.5) and Γ (0 0 0), in **k**-space for monoclinic and Γ (0 0 0), B (0.5 0.5 0), D (0.5 0 0.5), Z (0 0 0.5), Γ (0 0 0), Y (0 0.5 0), T (0−0.5 0), W (0 0.5 0) and Γ (0 0 0) for triclinic phases of the titled compound using PBE-GGA are illustrated in Fig. 2(a–d). The Fermi level is set to 0.0 eV Fig. 2(c,d) illustrated the band structures around E_F in the energy range between (−1.0 and 3.0) eV, it is clear that in the two phases the conduction band minimum (CBM) is located between D and Z points of the Brillouin zone while the valence band maximum (VBM) is located between Y and Γ points of the Brillouin zone, resulting in an indirect band gap. The calculated band gaps are found to be 1.884 eV (1.720 eV) using LDA and 1.935 eV (1.773 eV) using PBE-GGA for monoclinic (triclinic) phases, respectively. It can be noticed that moving from monoclinic to triclinic phase the CBM to shift towards lower energy by 0.162 eV resulting in a band gap reduction by around 0.162 eV. To the best of our knowledge, there is no previous report available in the literature (neither experimental data nor theoretical calculation for the energy band gap) to make a meaningful comparison.

3.2.2. Density of states

The total and partial density of states (DOS) were calculated by means of the modified tetrahedron method [29]. The input required for calculating the DOS are the energy eigenvalues and eigenfunctions which are the natural outputs of a band structure calculation. The total DOS and partial DOS are calculated for a large energy range (−8.34 eV up to 18.84 eV). The states below the Fermi energy (E_F) are the valence states and states above E_F are the conduction states. Hence we obtain DOS for both valence and conduction band states. The total density of states (TDOS) of both the monoclinic and triclinic phases are presented in Fig. 3. The figure shows that both phases show no significant variation in the density of states dispersion except some minor differences for instance, the structure in the occupied valence states between −7.0 and −5.0 eV of the monoclinic phase is relatively higher than that of the triclinic phase. The TDOS exhibits that the CBM of the triclinic phase shifts towards lower energy resulting in a band gap reduction, which confirms our previous observation from the calculated electronic band structure. The angular momentum decompositions of the atoms' projected density of states using PBE-GGA are presented in Fig. 4(a) and (b) for the monoclinic phase and in Fig. 4(c) and (d) for the triclinic phase. The occupied valence states for both phases are mainly produced by N-p, O-p and C-p with small contribution from

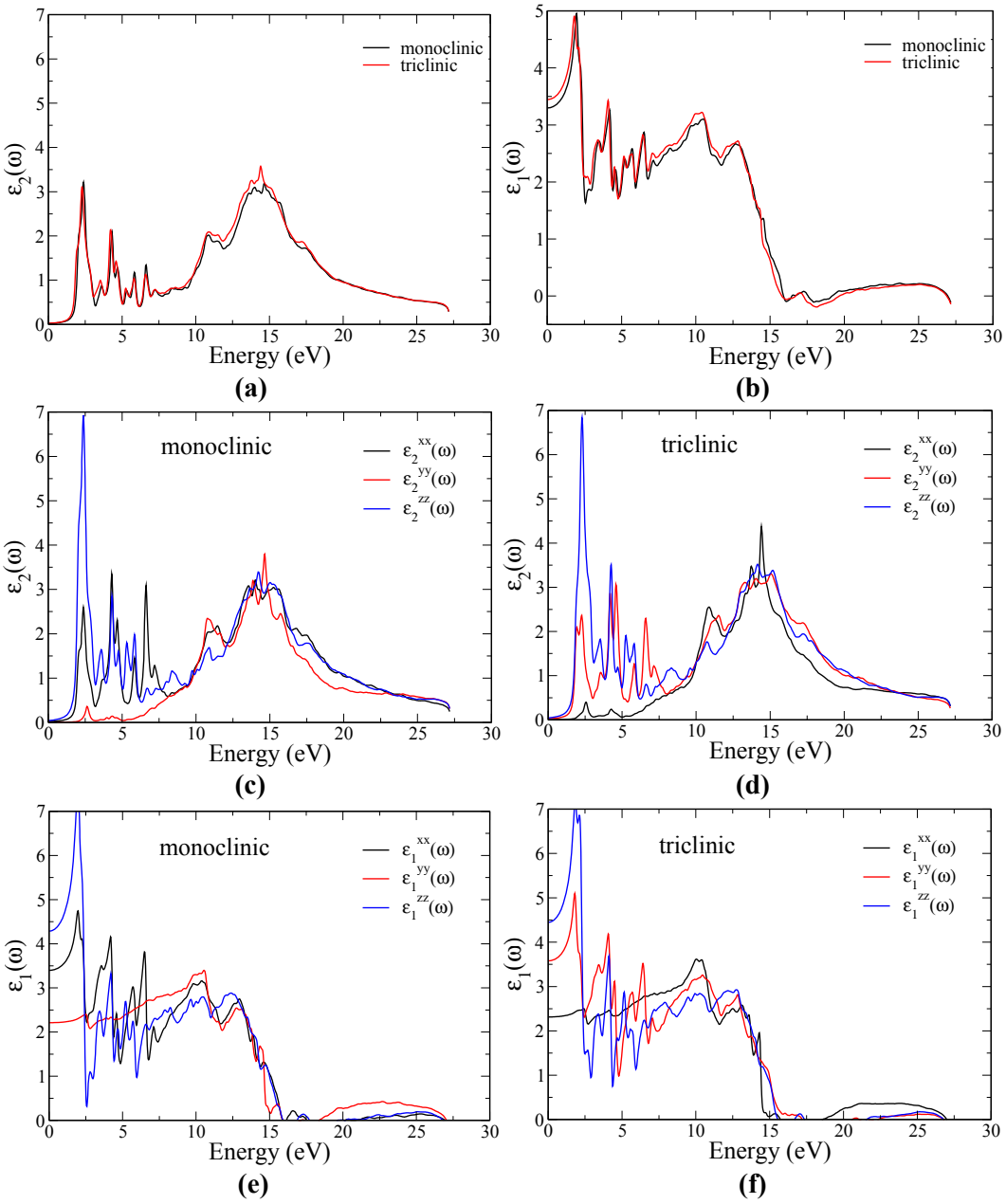

Fig. 6. The calculated $\varepsilon_2(\omega)$ dispersion spectra using PBE-GGA for (a) monoclinic phase and (b) triclinic phase. The calculated $\varepsilon_1(\omega)$ spectra using PBE-GGA for (c) monoclinic phase and (d) triclinic phase. These calculations were performed using PBE-GGA.

Table 1
Calculated $\varepsilon_1^{xx}(0)$, $\varepsilon_1^{yy}(0)$, $\varepsilon_1^{zz}(0)$, $n^{xx}(\omega)$, $n^{yy}(\omega)$, $n^{zz}(\omega)$ for monoclinic and triclinic phases using LDA and PBE-GGA.

	Monoclinic		Triclinic	
	LDA	GGA	LDA	GGA
$\varepsilon_1^{xx}(0)$	3.468	3.398	2.367	2.313
$\varepsilon_1^{yy}(0)$	2.263	2.212	3.687	3.579
$\varepsilon_1^{zz}(0)$	4.336	4.287	4.519	4.447
$n^{xx}(\omega)$	1.862	1.843	1.539	1.521
$n^{yy}(\omega)$	1.504	1.487	1.920	1.891
$n^{zz}(\omega)$	2.082	2.070	2.126	2.109

O-s, C-s and H-s for both the monoclinic and triclinic phases. It can be noticed that the amplitudes of C-s/p, N-p and O-p peaks are higher for the monoclinic phase. The conduction bands are mainly produced by N-s/p, O-p and C-p with a small contribution from O-s and C-s. There is a strong hybridization between N-p and O-p in the range from −9.0 to −8.0 eV and around 2.5 eV. In addition, we found that O-s state hybridized with C-s state in small energetic regions. The hybridization may lead to the formation of covalent bonding, the strength of the covalent bonding depends on the degree of the hybridization. In order to analyze the origin of chemical bonds between the atoms, the 2D charge-density contours are calculated in (1 0 0), (−1 0 1) and (0−1 1) crystallographic planes for the monoclinic and triclinic phases as shown in Fig. 5(a–f). According to the Pauling scale the electro-negativity of C, N, H and O atoms are 2.55, 3.04, 2.20 and 3.44, respectively. Therefore, if the electro-negativity difference between the atoms is greater than 1.7 the bonds exhibit predominantly ionic character,

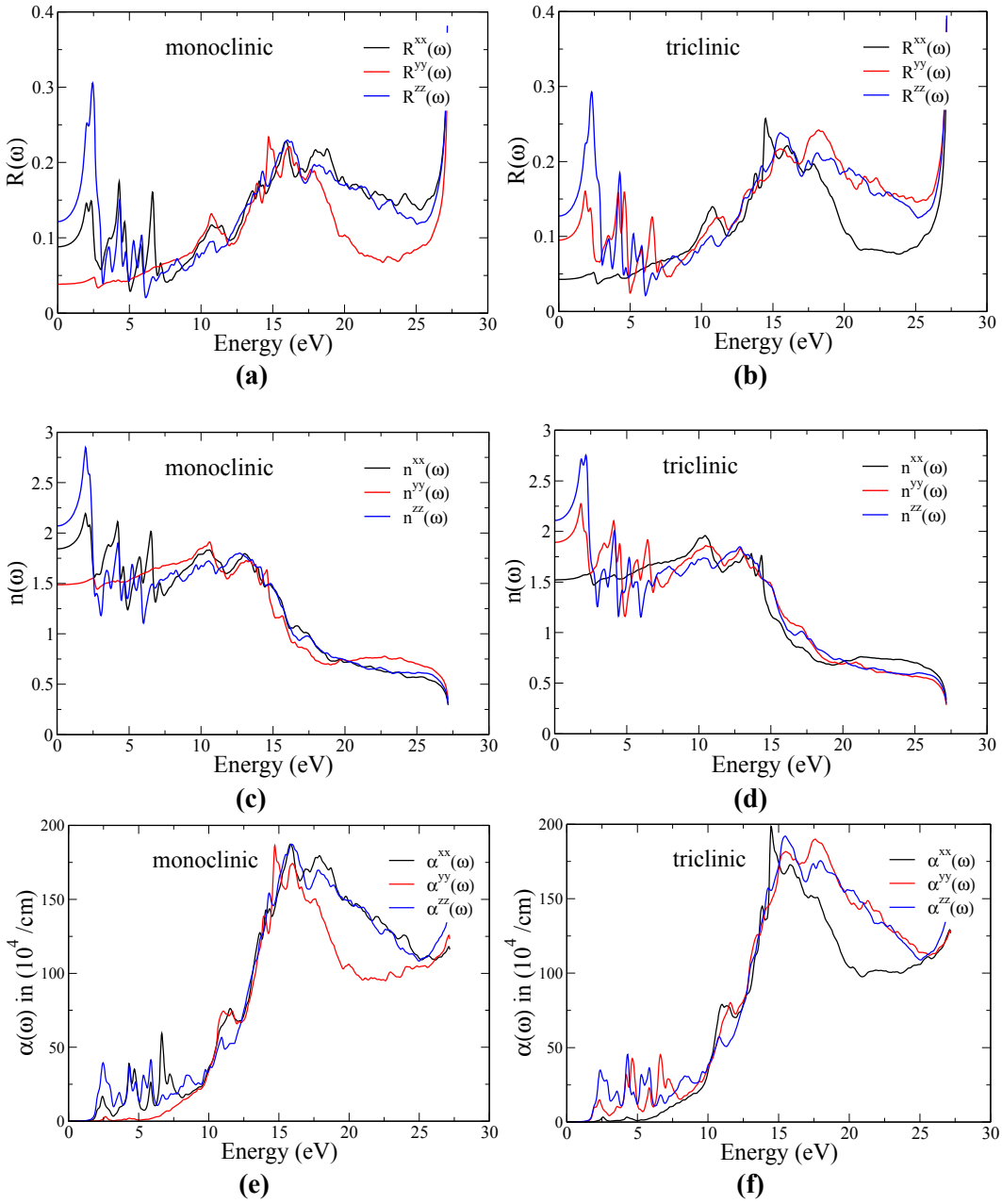

Fig. 7. The calculated R(ω) of the compound using PBE-GGA for (a) monoclinic phase and (b) triclinic phase. The calculated n(ω) spectra of the compound using PBE-GGA for (c) monoclinic phase and (d) triclinic phase. The calculated absorption spectra of the compound using PBE-GGA for (e) monoclinic phase and (f) triclinic phase. These calculations were performed using PBE-GGA.

while if the difference is less than 1.7 the bonds exhibit mainly covalent character, the less differences the stronger covalent bond. Hence, there exists a strong covalent bonding between C, N, H and O atoms. If we take a careful look at the (1 0 0), (−1 0 1) and (0−1 1) crystallographic planes we see that C atoms form strong covalent bond with N atoms. It has been found that the O atoms form strong covalent bonding with H, N and C atoms. Due to the high electronegativity of O and N atoms we can see charge transfer toward O and N atoms as indicated by the blue (blue in the web version) color according to the thermoscale. The thermoscale (see the thermoscale attached with the figures) indicated that the blue (blue in the web version) color exhibit the maximum charge. Similarly, from the thermoscale, we can see at the center of the hexagon (Fig. 5e and f) that there is zero charge as indicated by the red (red in the web version) color. Therefore, the calculated valence electronic charge density distribution helps to analysis the chemical bonding characters. In addition, we have calculated the bond lengths and angles as illustrated by Table S3−S8 (supplementary materials) in comparison with the experimental data [13], good agreement was found.

3.3. Optical properties

The average of the imaginary $\varepsilon_2^{average}(\omega)$ and real $\varepsilon_1^{average}(\omega)$ parts of the optical dielectric functions of the monoclinic and triclinic phases are illustrated in Fig. 6(a) and 6(b). It is clear that the

spectral structure of triclinic phase shifts towards lower energies confirming the gap reduction when we move from monoclinic to triclinic. The main spectral structures of $\varepsilon_2^{average}(\omega)$ are situated at around 2.5, 4.0 and 14.0 eV. The calculated $\varepsilon_1^{average}(0)$ confirms the gap reduction when we move from monoclinic to triclinic based on the Penn model [30]. Penn proposed a relationship between $\varepsilon_1(0)$ and the energy gap; the larger $\varepsilon_1(0)$ value corresponding to the smaller energy gap. This is further evidence that the phase transition cause a band gap reduction.

The principal components of the dielectric function along the polarization directions [100], [010] and [001] as shown in Fig. 6(c)-(f) exhibit a considerable anisotropy. At low energies around 2.5 eV we noticed that the optical component along the [001] polarization direction exhibit a major contribution to the optical spectra of both phases. It is interesting to highlight that the phase transition alters the spectral structure of optical components along the polarization directions [100] and [010] keeping the one along [001] unchanged as shown in Fig. 6(c) and (d). From the calculated $\varepsilon_1^{xx}(\omega)$, $\varepsilon_1^{yy}(\omega)$ and $\varepsilon_1^{zz}(\omega)$ we have obtained the vanishing frequency value of the dielectric function which defines the static electronic dielectric constant $\varepsilon_1^{xx}(0)$, $\varepsilon_1^{yy}(0)$ and $\varepsilon_1^{zz}(0)$. These values are listed in Table 1. The optical reflectivity of the monoclinic (triclinic) phases is presented in Fig. 7(a) (Fig. 7(b)), which shows that the optical reflectivity starts at about 12% (12.5%) for the *z*- (*z*-) component, 8% (9%) for the *x*- (*y*-) component and 3.5% (4.5%) for the *y*- (*x*-) component. The first reflectivity peak occurs at an energy level of about 2.5eV with reflectivity of 31% (29.5%) for the *z*-component, 15% (16%) for the *x*- (*y*-) component and 5% (5%) for the y- (x-) component. The first reflectivity maximum occurs at around 16.0 eV, at the energy where $\varepsilon_1^{xx}(\omega)$, $\varepsilon_1^{yy}(\omega)$ and $\varepsilon_1^{zz}(\omega)$ crosses zero (Fig. 6(b), (e) and (f)) which is associated with the existence of plasma oscillations. In Fig. 7(c) and (d) the refractive indices of the two phases are plotted as a function of energy. The calculated values of $n^{xx}(0)$, $n^{yy}(0)$ and $n^{zz}(0)$ are listed in Table 1, we found that these values are higher for the triclinic phase. From these values we can obtain the value of the energy gap, both of $\varepsilon_1(0)$ and $n(0)$ (n=ε) are inversely proportional with the energy gap. This is further evidence that the phase transition causes a band gap reduction.

The calculated absorption coefficient $I(\omega)$ of the monoclinic (triclinic) phases is presented in Fig. 7(e) (Fig. 7(f)). It shows the fundamental optical absorption edges situated at 1.935 eV (1.772 eV) using PBE-GGA. It has been noticed that $I^{xx}(\omega)$, $I^{yy}(\omega)$ and $I^{zz}(\omega)$ of both phases increases drastically after the fundamental optical absorption edges. We should emphasize that monoclinic and triclinic phases exhibit a wide optical transparency region up to 1.8835 eV ($\lambda = 6408$ Å) and 1.773 eV ($\lambda = 6993$ Å), respectively. To the best of our knowledge there has been no previous data on the optical properties for these two phases reported in the literature. Thus, this work can assist as reference data for the optical properties of this compound.

4. Conclusions

We have investigated the structural, electronic, and optical properties of the $(C_6H_{13}N_4^+ \cdot C_6H_3N_2O_5^- \cdot H_2O)$ compound in monoclinic and triclinic phases using the FP-LAPW + lo method as implemented in the WIEN2k package, based on the density functional theory. The optimized atomic geometry shows a good agreement with the experimental data. The band gaps were calculated for the two phases using LDA and PBE-GGA, and we found that these phases possess an indirect band gap. It has been found that the phase transition (monoclinic → triclinic) causes a band gap reduction by around 0.162 eV. The density of states implies that weak/strong hybridization exists between the states. The hybridization may cause covalent bonding depending on the degree of the hybridization. The calculated valence electronic charge density reveals that there exists a strong covalent bonding between C, N, H and O atoms. The calculated optical properties confirm the band gap reduction during the phase transition. It also shows the existence of the considerable anisotropy between the optical components along the three polarization directions. It is interesting to highlight that the monoclinic and triclinic phases exhibit a wide optical transparency region up to 1.8835 eV ($\lambda = 6408$ Å) and 1.773 eV ($\lambda = 6993$ Å), respectively.

Acknowledgments

This project was supported by the Research Center, College of Science, King Saud University. A. H. Reshak would like to acknowledge the CENTEM project, reg. no. CZ.1.05/2.1.00/03.0088, cofunded by the ERDF as part of the Ministry of Education, Youth and Sports OP RDI programme and, in the follow-up sustainability stage, supported through CENTEM PLUS (LO1402) by financial means from the Ministry of Education, Youth and Sports under the National Sustainability Programme I. Computational resources were provided by MetaCentrum (LM2010005) and CERIT-SC (CZ.1.05/3.2.00/08.0144) infrastructures.

Appendix A. Supplementary data

Supplementary data related to this article can be found at http://dx.doi.org/10.1016/j.matchemphys.2015.12.063.

References

[1] Agency for Toxic Substances and Disease Registry (ATSDR), Toxicological Profile for Dinitrophenols, Public Health Service, U.S. Department of Health and Human Services, Atlanta, GA, 1995.
[2] J. Grundlingh, P.I. Dargan, M. El-Zanfaly, D.M. Wood, 2,4-Dinitrophenol (DNP): a weight loss agent with significant acute toxicity and risk of death, J. Med. Toxicol. 7 (2011) 205–212.
[3] J.A. Harper, K. Dickinson, M.D. Brand, Mitochondrial uncoupling as a target for drug development for the treatment of obesity, Obes. Rev. 2 (2001) 255–265.
[4] E. Colman, Dinitrophenol and obesity: an early twentieth-century regulatory Dilemma, Regul. Toxicol. Pharmacol. 48 (2007) 115–117.
[5] A. Tewari, A. Ali, A. O'Donnell, M.S. Butt, Weight loss and 2,4-dinitrophenol poisoning, Br. J. Anaesth. 102 (2009) 566–567.
[6] F. Devlieghere, L. Vermeiren, M. Jacobs, J. Debevere, The effectiveness of hexamethylenetetramine-incorporated plastic for the active packaging of foods, Packag. Technol. Sci. 13 (2000) 117–121.
[7] H. Miller, E. Phillips, Antibacterial correlates of urine drug levels of hexamethylenetetramine and formaldehyde, Investig. Urol. 8 (1970) 21–33.
[8] C.W. Bedford, Art of vulcanizing caoutchouc, U. S. Pat. Off. US1418772 A (1922).
[9] R.L. Sibley, N.W. Va, Art of vulcanizing rubber, U. S. Pat. Off. U. S. 1998559 A (1935).
[10] Martindale, The Extra Pharmacopoeia, 30th edition, 1993, p. p173.
[11] H.-K. Fun, A. Usman, S. Chantrapromma, J. Osman, L.-H. Ong, D.R. Tilley, Y. Ishibashi, Phase transitions in hydrogen-bonded phenol–amine adducts: analysis by ferroelastic theory, Solid State Commun. 127 (2003) 677–682.
[12] R. Purohit, P. Venugopalan, Resonance 14 (2009) 882–893.
[13] A. Usman, S. Chantrapromma, H.-K. Fun, Acta Crystallogr. Sect. C57 (2001) 1443–1446.
[14] H.-K. Fun, A. Usman, S. Chantrapromma, J. Osman, L.-H. Ong, D.R. Tilley, Y. Ishibashi, Solid State Commun. 127 (2003) 677–682.
[15] P.T. How, B.S. Lee, H.-K. Fun, I.A. Razak, S. Chantrapromma, Phys. Rev. B 71 (2005) 174109–174121.
[16] H.-K. Fun, B.S. Lee, S. Chantrapromma, Ferroelectrics 349 (2007) 45–48.
[17] S. Chantrapromma, H.-K. Fun, A. Usman, J. Mol. Struct. 789 (2006) 30–36.
[18] H.-K. Fun, M.M. Rosli, B.-S. Lee, L.-H. Ong, S. Chantrapromma, J. Mol. Struct. 837 (2007) 132–141.
[19] H.-K. Fun, C.K. Quah, S.R. Jebas, L.-H. Ong, J. Mol. Struct. 964 (2010) 31–38.
[20] C.K. Quah, H.-K. Fun, L.-H. Ong, J. Mol. Struct. 1010 (2012) 8–16.
[21] P. Blaha, K. Schwarz, G.K.H. Madsen, D. Kvasnicka, J. Luitz, WIEN2k, an Augmented Plane Wave−+−Local Orbitals Program for Calculating Crystal Properties (Karlheinz Schwarz, Techn. Universitat Wien, Austria), 2001, ISBN 3-9501031-1-2.
[22] W. Kohn, L.J. Sham, Phys. Rev. 140 (1965) A1133–A1138.
[23] J.P. Perdew, A. Zunger, Phys. Rev. B 23 (1981) 5048.
[24] J.P. Perdew, K. Burke, M. Ernzerhof, Phys. Rev. Lett. 77 (1996) 3865.

[25] C. Ambrosch-Draxl, J.O. Sofo, Linear optical properties of solids within the full-potential linearized augmented planewave method, Comput. Phys. Commun. 175 (2006) 1–14.
[26] http://www.wien2k.at/reg_user/textbooks/usersguide.pdf.
[27] http://plasma-gate.weizmann.ac.il/Grace/and http://exciting-code.org/xmgrace-quickstart.
[28] http://www.linuxquestions.org/questions/linux-software-2/installing-xcrysden-4175449852/.
[29] P.E. Blöchl, O. Jepsen, O.K. Andersen, Phys. Rev. B 49 (1994) 16223–16233.
[30] D.R. Penn, Phys. Rev. 128 (1962) 2093–2097.